High-resolution 3D hyperspectral digital surface models from lightweight UAV snapshot cameras – potentials for precision agriculture applications

Helge Aasen

GIS and Remote Sensing Research Group, Institute of Geography, University of Cologne, Cologne, Germany

A paper from the Proceedings of the
13th International Conference on Precision Agriculture
July 31 – August 4, 2016
St. Louis, Missouri, USA

Abstract. *Precision agriculture applications need timely information about the plant status to apply the right management at the right place and the right time. Additionally, high-resolution field phenotyping can support crop breeding by providing reliable information for crop rating. Flexible remote sensing systems like unmanned aerial vehicles (UAVs) can gather high-resolution information when and where needed. When combined with specialized sensors they become powerful sensing systems.*

Hyperspectral data has been shown to provide information about biophysical and biochemical properties of vegetation and agricultural crops, for biotic and abiotic stress detection and biomass and yield estimation. Recently, lightweight hyperspectral snapshot cameras have been introduced, which record spectral information as a two dimensional image with every exposure. Specialized workflows based on photogrammetric algorithms allow reconstructing the 3D topography of a surface from this data and thus retrieve structural and spectral information at the same time.

Hyperspectral digital surface models (HS DSMs) derived from snapshot cameras are a novel representation of the surface in 3D space linked with spectral information about the reflection and emission of the objects covered by the surface. In this contribution the requirements and workflow to derive HS DSM of crop canopies are described and their potential for precision agriculture applications is demonstrated. The data is derived by the hyperspectral snapshot camera UHD 185 – Firefly, which records hyperspectral information from 450 to 950 nm in 138 bands

Results from a multi-temporal monitoring campaign of an experiment with two nitrogen fertilizer treatments and six different spring barley cultivars are presented. The campaign was carried out at

the research station Campus Klein-Altendorf, belonging to the University of Bonn, close to the city of Bonn, Germany. From the HS DSM the chlorophyll content, plant height and biomass were estimated for individual growth stages and across several growth stages. Plant height was estimated with an R^2 of up to 0.98, chlorophyll with R^2 of 0.13 to 0.64 depending on the growth stage. Additionally, based on three years of experience with hyperspectral UAV snapshot cameras important remarks regarding the 3D and spectral data quality are given.

Keywords. *Hyperspectral, barley, field-phenotyping, unmanned aerial vehicle, remotely piloted aircraft systems, Unmanned Aerial System, chlorophyll, plant height, structure from motion, photogrammetry, digital surface model, canopy height, red-edge inflection point*

Introduction

Global agriculture faces enormous challenges. The world's population is growing and large parts of it are changing their diet to an increased consumption of high-protein and energy-dense food such as meat (Pingali, 2007). At the same time, there are approximately 870 million people worldwide who are undernourished (FAO, 2012). Thus, global crop production will need to be doubled by 2050 (Tilman et al., 2011). In light of the planet's limited resources and increasing global population, a turn is needed towards more sustainable growth in agricultural production while simultaneously diminishing its environmental footprint (Foley et al., 2011).

One approach towards more sustainable crop production is increasing the cropping efficiency (Foley et al., 2011). This can be accomplished by dividing agricultural areas into management zones that receive customized management inputs based on crop requirements as they vary in the field, such that resources are used in the right place at the right time. Such practices are called site-specific crop management (Pinter et al., 2003; Whelan and Taylor, 2013) and are part of precision agriculture (Mulla, 2013). However, the operational success of variable applications of fertilizer or other management actions requires accurate data to produce maps of crop growth, weeds, insect infestations, nutrient and water deficiencies and other crop and soil conditions (Moran et al., 1997). The timeliness of that information is important. Phenomena such as plant diseases are highly dynamic and require short revisit times (Voss et al., 2010).

Hyperspectral data has been shown to provide information about biophysical and biochemical properties of agricultural crops such as biomass (Aasen et al., 2014; Gnyp et al., 2013; Marshall and Thenkabail, 2015), LAI (Broge and Leblanc, 2001; Haboudane et al., 2004), chlorophyll (Aasen et al., 2015; Daughtry et al., 2000; Haboudane et al., 2002; Yu et al., 2014) or nitrogen (Inoue et al., 2012; Li et al., 2010). Additionally, it has been used to detect biotic and abiotic stress (Elsayed et al., 2015; Mahlein, 2016; Yu et al., 2013). Also, it has been used in the context of precision agricultural applications (Yao et al., 2012). Commonly, ground-based spectral measurements are carried out with field-spectrometers to study "the interrelationships between the spectral characteristics of objects and their biophysical attributes in the field environment" to "act as a bridge between laboratory […] and field situations" and "provide a tool for the development, refinement and testing of models relation biophysical attributes to remotely-sensed data" (Milton, 1987). To cover larger areas imaging spectroscopy system are used to generate a representation of the spectral properties of a surface in two spatial dimensions. Most imaging systems scan the surface point- (whiskbroom) or line-wise (pushbroom). In both cases, a 2D representation of the surface is built up while the sensor is moving across the surface (or an object is moved by the sensor, e.g. on a conveyer belt). These systems are mostly applied from aircrafts or satellites. Current satellite systems allow capturing spectral information in a spatial resolution of up to 1.3 m (e.g. WorldView-3; DigitalGlobe, 2016), while freely available spectral information has a resolution of up to 10 m (Sentinel-2; ESA, 2016). However, current agricultural machinery allow to apply crop treatments with a spatial resolution of approximately 0.25 m (e.g. Leeb GS; HORSCH Maschinen GmbH, 2016). Thus, spectral data with a higher spatial resolution would be beneficial to explore the full potential of these machines. Additionally, the temporal resolution of geospatial information acquired by satellite based remote sensing systems is compromised by cloud cover, orbiting time and scene availability (Aasen, in review).

Besides, structural information, such as the plant height, may provide complementary information about the crops status. Plant height alone (Bendig et al., 2014; Ehlert et al., 2008; Pittman et al., 2015; Tilly et al., 2014) and in combination with spectral information (Bendig et al., 2015; Marshall and Thenkabail, 2015; Tilly et al., 2015) has been used to estimate biomass, water stress (Baher et al., 2002) and yield (Geipel et al., 2014).

In the last 10 years or so, 'Unmanned Aerial Vehicles' (UAVs), also known as 'Unmanned Aerial Systems' or 'Remotely-Piloted Aerial Systems', have infiltrated the field of remote sensing as a new sensing platform. Small consumer-grade UAVs are rather low-cost platforms and operationally

flexible (Berni et al., 2009), which makes them suitable for a number of applications including precision farming (for a comprehensive overview please refer to Colomina and Molina, 2014; Pajares, 2015; Salamí et al., 2014). Additionally, they can fly slowly at low altitudes and are able to acquire spatial information in high resolution (Pajares, 2015). Together with specialized sensors, they are becoming powerful sensing systems (Aasen and Bolten, in review).

Recently, hyperspectral snapshot cameras (HSCs) have been introduced to remote sensing (Aasen et al., 2015; Aasen and Bolten, in review). HSCs record spectral information in two spatial dimensions within a single exposure and therefore without any scanning process (Hagen et al., 2012). In contrast to whisk- or pushbroom spectrometers, snapshot cameras (also called central perspective imagers) capture a 2D image at one instant of time from the viewpoint of the camera lens (Jones and Vaughan, 2010). Consequently, in case of spectral snapshot cameras a full image cube is recorded within one integration of the sensor. Thus, a movement of the sensing system can be used to create multiple overlapping image cubes (Figure 1).

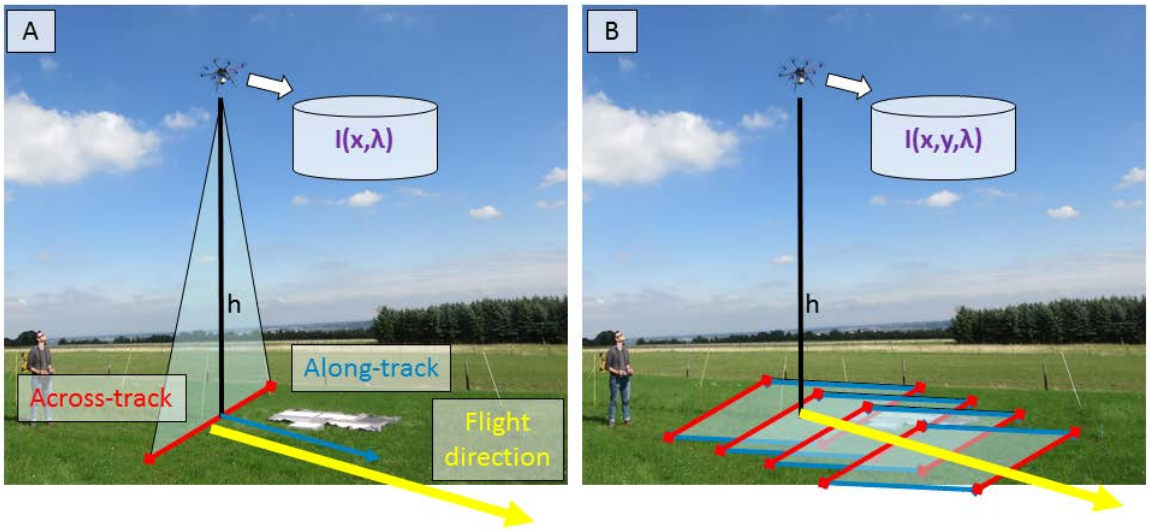

Figure 1 Different principles of data acquisition. Line-scanning devices record individual image-lines along one spatial dimension. Movement of the sensing system is needed to create a 2D scene (A). Snapshot cameras record image cubes with two spatial dimensions with every exposure. Thus, movement generates overlapping image cubes (B) (Aasen, in review).

This enables a new approach to capture information about agricultural crops by utilizing advances in the field of robotics, sensor technology, computer vision and photogrammetry: Hyperspectral digital surface models (HS DSMs) generated with UAV snapshot cameras are a representation of a surface in 3D space linked with hyperspectral information emitted and reflected by the objects covered by that surface. In the following, these HS DSMs are introduced and their potential for precision agriculture applications by means of a multi-temporal field study within a barley phenotyping experiment with different barley varieties and different fertilization levels is investigated. Results from the estimation of chlorophyll and plant height from the HS DSMs are shown. Additionally, based on three years of experience challenges during the acquisition and data processing procedure are identified.

Materials and methods

Study site

The study was carried out at the research station Campus Klein-Altendorf (50° 37′51″N, E 6°59′32″) of the University of Bonn (https://www.cka.uni-bonn.de/) at a field experiment of the interdisciplinary research project CROP.SENSe.net (www.cropsense.uni-bonn.de) in 2014. The soil was a clayey silt luvisol. The campus-owned weather station reported a long-term average precipitation of 600 mm

and a daily average temperature of 9.3 °C for 2014 (Campus Klein-Altendorf, 2010). 36 plots of different spring barley cultivars were sampled. Half of them were treated with a farmer's common rate of 80 kg/ha nitrogen (N) fertilizer and the other half with 40 kg/ha N. Six cultivars (Barke, Beatrix, Eunova, Trumpf, Mauritia and Sebastian) in three repetitions were sampled (Aasen, in review). The experiment is shown in Figure 2. The size of each experimental plot was 3 x 7 m. Each plot was divided into two parts: in one part, destructive measurements of chlorophyll was carried out. In the remaining part, non-destructive remote sensing and plant height measurements were taken. To exclude border effects a 0.8 m distance to the plot border was kept. The plots were separated by paths of bare soil. Four flight campaigns were carried out at 56, 70, 84, 96 days after seeding (DAS). The plant height and chlorophyll measurements were carried out simultaneously. Chlorophyll was measured by collecting four samples of leafs at the top layer of the canopy. These were instantly frozen with liquid nitrogen inside a dryshipper to preserve the samples. Later the chlorophyll content was measured with the DMSO-Method (Blanke, 1992) at the Institute of Crop Science and Resource Conservation (INRES), University of Bonn.

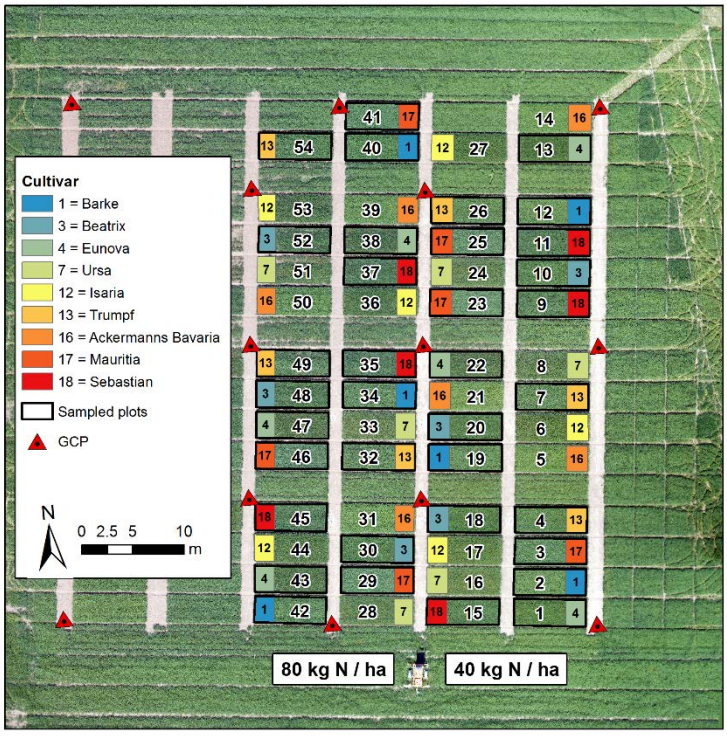

Figure 2 Map of the CROP.SENSe.net experiment at Campus Klein-Altendorf in 2014 with plot number (large numbers) and cultivar (small numbers). The cultivar-wise colored squares indicate the destructive measurement part. The destructively sampled plots are framed with a solid rectangle. Positions of the ground control points (GCPs) and terrestrial laser scanning positions (TLS) are shown. The two plot rows to the left were treated with a farmer's common rate of 80 kg/ha nitrogen (N) fertilizer and the other half with 40 kg/ha N (adapted from Aasen, in review).

Sensing system

Our carrier platform MK-OktoXL (http://www.mikrokopter.de) is a rotary-wing UAV with a maximum payload of 2.5 kg (Figure 3.1). Depending on the payload and the batteries, the flight time varies from 15 to 30 min. The altitude, speed and position is controlled during the flight and logged to an on-board memory card. The flight path is controlled by the autopilot Flight Ctrl. 2.1 following predefined waypoints configured in the MikroKopterTool. The payload is mounted on a gimbal. We use the MK HiSight SLR2 gimbal that compensates for pitch and roll movement during the flight by using the UAV's on-board gyroscopes. The compensation allows to maintain a nadir orientation of the sensor. The weight of the gimbal is about 280 g.

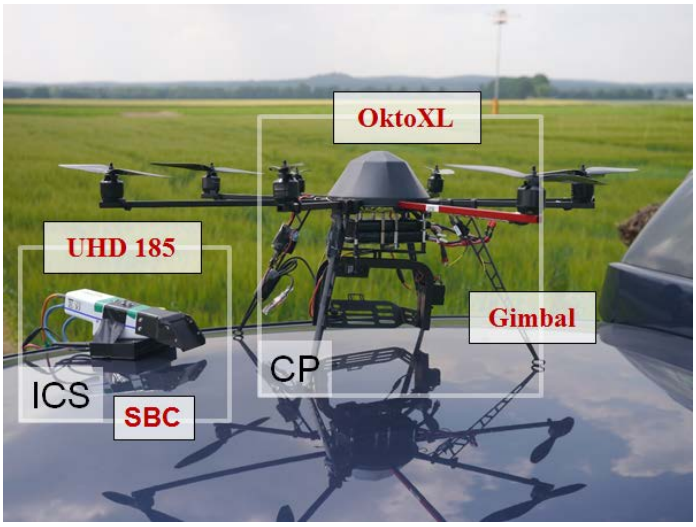

Figure 3 Carrier Platform (CP) MikroCopter Okto XL with Gimbal and image capturing system (ICS) with UHD 185-Firefly and the single board computer (SBC) Pokini Z (Aasen et al., 2015).

Our image capturing system consists of the Cubert UHD 185-Firefly (UHD) HS snapshot camera and the small single board computer (SBC) Pokini Z (http://www.pokini.de/). The UHD simultaneously captures 138 spectral bands with a sampling interval of 4 nm. From these bands the camera's manufacturer recommends the use of 125 bands between 450 and 950 nm. The FWHM of the bands increases from about 4 nm at 450 nm to about 26 nm at 850 nm. For each band a 50 by 50 pixel image with 12 bit (4096 DN) dynamic range is created. At the same time as the HS image is recorded, a grayscale image with a resolution of 990 by 1000 pixel is captured. We use a lens with a focal length of 16 mm resulting in an across track field of view (FOV) of approximately 20°. Since the camera's housing is elongated with the lens looking forward a mirror is fixed at the front to capture nadir images (Figure 3.1). The ground resolution at 30 m flying height is about 21 cm for the HS pixels and 1 cm for the grayscale image. The total weight of the Camera is about 470 g. and its housing is about 28 by 6.5 by 7 cm. The camera is controlled by a SBC. The performance of the SBC allows to capture HS image cubes with a frame rate of about 0.6 hertz. The typical integration time under cloudless conditions is 1 ms, increasing to about 6 ms under cloud covered conditions. The whole image capturing system together with a three cell lithium polymer battery weighs about 1 kg (Aasen et al., 2015).

Data proessing and hyperspectral digital surface model generation

Before each flight, a reference image was taken by placing the camera and UAV above a white calibration panel (Zenith Lite). After dark current correction, this image was used to convert the raw digital numbers of each image taken during the flight to reflectance. This spectral information was merged with the high-resolution grayscale image into an image cube and information about the pixel position within the image was appended as introduced by Aasen et al. (2015). The individual image cubes were loaded into Photoscan (Professional Edition, version 1.1.6, www.agisoft.com) and processed with the typical workflow: after initial photo alignment, the scene was georeferenced by all GCPs visible in the scene and a dense point cloud (ultra-high) was created. At this stage, an HS dense point cloud was created. Thus, in contrast with traditional approaches, the HS and 3D information is linked inherently throughout the processing and no further post-processing is needed. The hyperspectral and 3D spatial was exported with a spatial resolution of 5 cm. The resulting HS DSM contained a representation of the 3D surface linked with hyperspectral information emitted and reflected by the objects covered by the surface (Aasen et al., 2015).

Plant height extraction

The height in the HS DSM represents as the absolute height above the ellipsoid. The difference

between the DSM and the digital terrain model (DTM), which is the height of the bare soil surface, represents the crop height. To calculate this height a DTM was generated from the non-vegetated paths between the experimental plots for each date: DTM extraction points were placed every 3 m and the height of a circle with a radius of 0.2 m around the points was averaged to minimize small scale differences of the bare soil. Based on these values a DTM was interpolated. From the DSM the generated DTM was subtracted. The result represents the average height of the plants within a pixel. This height will be referred to as canopy or crop height model (CHM). For each plot the average height of the CHM was extracted from the non-destructive measurement part of the plot with a margin of 0.8 m to the plot border to exclude influences of tractor tracks and border effects (Figure 4).

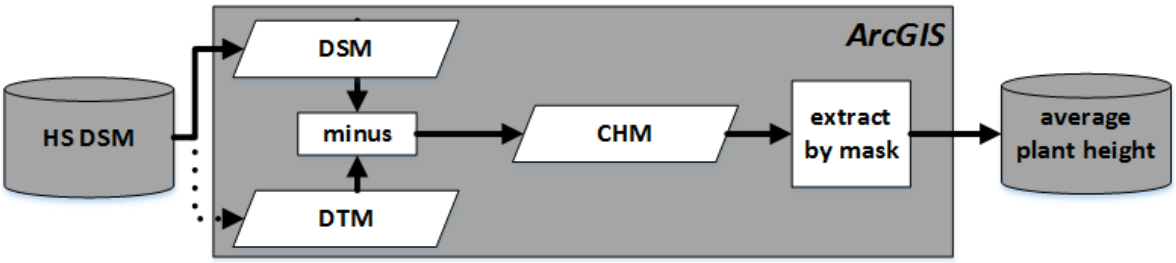

Figure 4 Plant height extraction from the hyperspectral digital surface model (HS DSM). A digital terrain model (DTM) is created and subtracted from the digital surface model. The result is a canopy height model (CHM).

Besides the image overlap, the number and placement of GCPs influences the quality of a surface derived from SfM (Harwin and Lucieer, 2012; Mesas-Carrascosa et al., 2015). DSM from SfM are prone to the 'bowl effect' which occurs when the area mapped exceeds the area surrounded by GCPs (Ouédraogo et al., 2014). In our dataset, only the HS DSMs of the first date covered the entire extent of the experimental area. For DAS 70 and DAS 84, the GCPs were missing on the east side of the covered area. To counteract the 'bowl effect', the DTMs were generated individually for each date. Also, plots that were not entirely covered by the generated DTM were excluded. For DAS 70, the most western row was excluded from the analysis as an additional case (DAS 70b), since this area had low image overlap in the HS DSM.

The plant height derived from the HS DSM was compared to ruler measured plant heights. Within each plot, the height of ten individual plants was measured and the median was calculated. From the HS DSM the average height per plot was calculated. These estimates where compared for each date and across all dates.

Chlorophyll retrieval

To evaluate the estimation of chlorophyll the red-edge inflection point (REIP; Guyot and Baret, 1988) was used. For each pixel the REIP was generated and all pixels (with a 0.8 m border) from the non-destructive part of the plot were averaged to represent a plot. A linear regression model was established for the data of each individual date.

Results

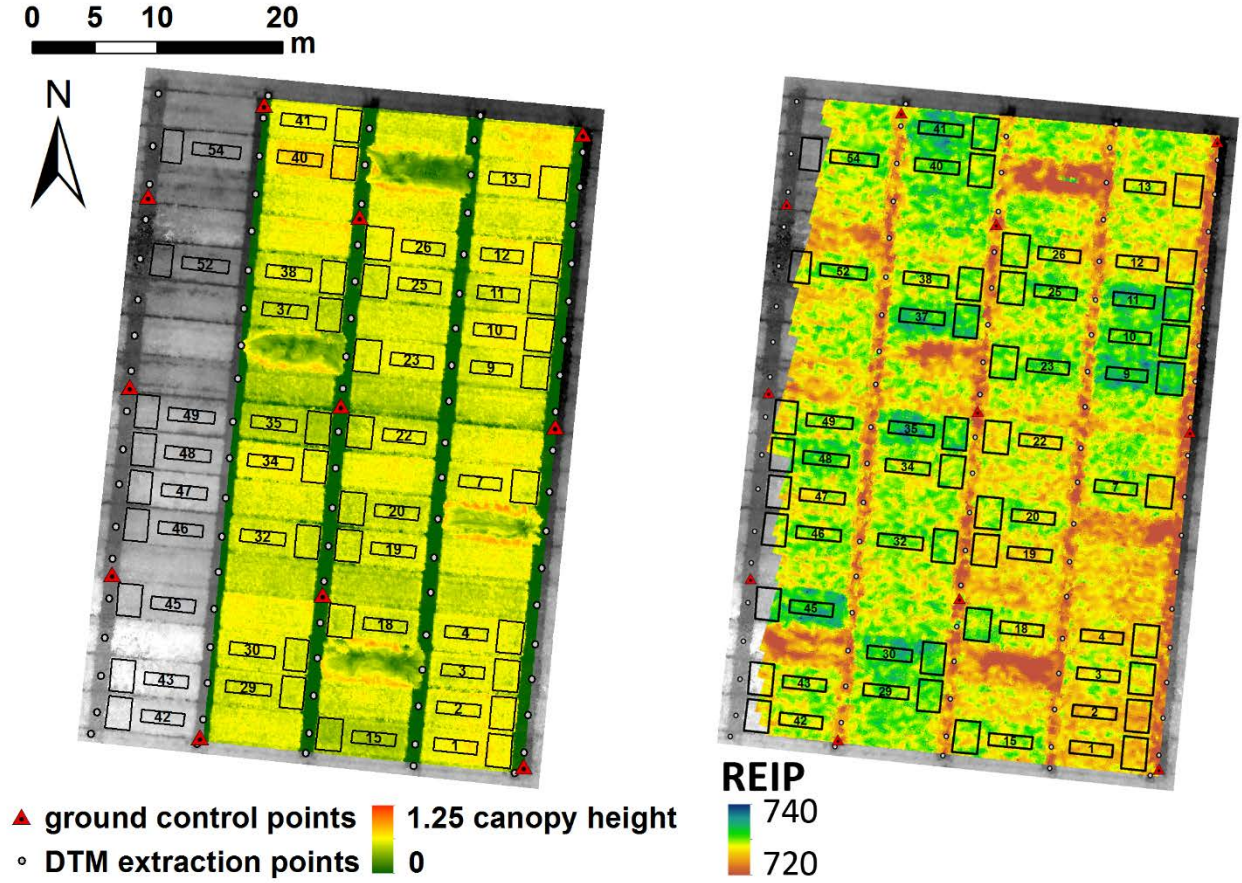

Figure 5 Map of the plant height (left) and red-edge inflection point (right) at 96 days after seeding. Four plots have experienced lodging. For the most western row the image overlap was not sufficient to generate a digital surface model.

Figure 5 shows maps of the plant height (left) and REIP (right) derived from the HS DSM at 96 DAS. In the plant height map the tracks of bare soil in between the experimental plots are visible. Additionally, lodging of four plots is visible. These belong to the cultivar Isaria. Besides, also slight differences between the different cultivars are visible. In the REIP map, differences between the cultivars are more pronounced. In particular, the varieties Sebastian (plot 9, 11, 35, 37, 45), Mauritia (plot 3, 23, 25, 29, 41, 46) and Beatrix (plot 10, 18, 20, 30, 48, 52) stand out with high REIP values. Similar to the plant height, the lodged plots are visible in the spectral data. Additionally, also within-plot heterogeneity is visible both in the spectral and the plant height maps.

To evaluate the quality of the plant height derived from the HS DSM it was compared to manual ruler measured plant heights. Figure 6 shows the scatterplot for the individual dates and all dates together. An increase in plant height is visible until DAS 84. The relationships between the ruler measurements and the HS DSM derived plant heights are quantified in Table 1.

Table 1 Quantitative comparison of the ruler measured and the HS DSM derived plant heights.

DAS	56	70	70b	84	96	56 - 84	All
R^2	0.83	0.35	0.70	0.81	0.45	0.98	0.96
RMSE (m)	0.06	0.12	0.08	0.09	0.17	0.12	0.20
RMSE (%)	16	20	13	11	22	20	32
slope	0.66	0.48	0.89	0.89	0.97	0.71	0.75
mean difference	0.11	0.15	0.25	0.26	0.19	0.16	0.17

DAS 56, 84 and the multi-date sets achieve $R^2 > 0.8$. DAS 70 and 96 achieve lower relations. When plots 41 – 54 are excluded from the DAS 70 dataset (DAS 70b) the R^2 increases to 0.7 and the relative RMSE decreases to 12 %. Overall, the RMSE is between 11 and 22% for the single dates and at 32% for all dates together. The slope of the regression line is between 0.66 for DAS 56 and 0.97 for DAS 96. For all dates, the HS DSM derived plant height is lower than the ruler measured plant height. The mean difference varies from 0.11 m for DAS 56 to 0.26 m for DAS 84. The quality of the spatial information in the HS DSM also influences the retrieval of the plant height. This can be seen in the significantly increased R^2 and the slope of the regression when the most western row at DAS 70 is excluded. As mentioned above, the image coverage and especially the across track image overlap in this part of the scene was very limited so that the CHM bended downwards at the bare soil path to the west side of the model and upwards in the area of the plot. Thus, these plots showed a higher plant height in the CHM relative to the other plots for the date (Figure 6, brown dots).

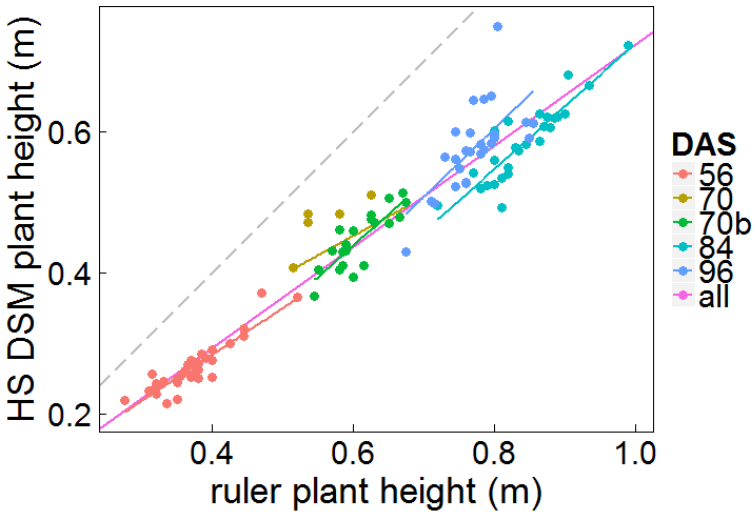

Figure 6 Scatterplot of the ruler and HS DSM derived plant heights for the individual four measurement dates at 56, 70, 84 and 96 days after seeding (DAS), and DAS 70 without plot 46 – 54 (green) and all dates together (pink). The one to one line is shown in gray.

With the ruler, the heights of individual plants within the plot are measured. On the contrary, the very high-resolution point cloud, from which the HS DSM is derived, does not only represent the highest parts of plants but also reflects heterogeneity in conjunction with the canopy structure. Thus it approximates an average canopy height lower than the ruler derived plant heights. This is also supported by a study by Tilly et al. (2015), where a maximum point filter was used to derive the plant height and a similar offset could not be observed. The slope, close to 1 in most cases, demonstrates the feasibility to estimate the plant height both for individual dates and across several growth stages. However, the best data processing scheme to derive a specific parameter needs further investigation. The latter might also depend on the application, since for some applications the maximum plant height might be interesting (e.g. stem growth rate), while for others an average

canopy height might be beneficial (e.g. biomass estimation).

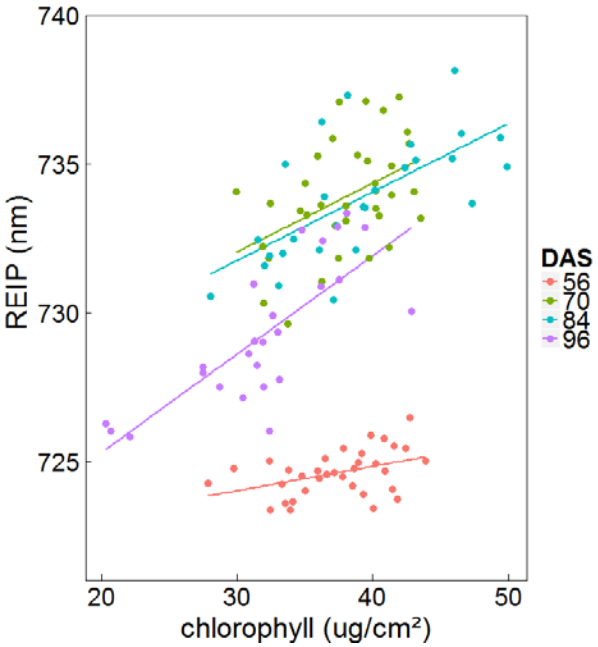

Figure 7 Scatterplot of the REIP with chlorophyll for 56, 70, 84, 96 days after seeding (DAS).

Figure 7 shows the scatterplot for the REIP and chlorophyll for four different DAS. The chlorophyll values for DAS 56 and 70 are within the same range. Still, the REIP values for DAS 56 are significantly lower than for the other DAS. DAS 96 has the widest spread of chlorophyll and REIP values. For DAS 56 and 70 only low coefficients of determination are achieved with the REIP. For DAS 84 and 96 chlorophyll can be predicted with an R^2 of above 0.44 (Table 2).

Table 2 Coefficients of determination between the red-edge inflection point (REIP) and destructively measured chlorophyll for 56, 70, 84, and 96 days after seeding (DAS).

DAS	56	70	84	96
REIP	0.18	0.13	0.44	0.60

Discussion

As seen at DAS 70 a high image overlap is critical to achieve a good DSM and consequently, good results for the plant height. Insufficient overlap can result in a bended 3D model and thus, in wrong plant height estimations. Additionally, ideally the coverage of the images should extent the area of interest and GCPs should be placed around and ideally within the area of interest to prevent the 'bowl-effect' (Aasen, in review; Ouédraogo et al., 2014). This can be seen in the DSM of DAS 70 (Figure 8), where approximately the half of the most western row is very noisy and tilts. Thus, excluding the affected plots increases the correlation with the manual measured plant heights (case 70b, cf. Table 1 and Figure 6). Typically, an overlap of 60% across and 80% along track is recommended (Agisoft LLC, 2016). In this contribution, Photoscan was used to reconstruct the 3D information. It should be noted that significant differences exist between different software packages (Eltner and Schneider, 2015; Gómez-Gutiérrez et al., 2014; Grenzdörffer, 2014; Remondino et al., 2014). Additionally, the flight pattern and illumination conditions during the flight may influence the resulting 3D point cloud (Dandois et al., 2015). But also point clouds derived with different active or passive sensing systems, such as Light detection and ranging devices or cameras with different resolutions, may differ (Aasen, in review; Dandois and Ellis, 2010). Thus, results derived with different processing workflows might not be comparable 'per se'. Consequently, if measurements undertaken with different systems, processing workflows or under changing conditions are to be

compared, the measurement circumstances and processing workflows need to be carefully described. Additionally, more research on the systematic differences between the different approaches is needed. Besides, the high resolution of the 3D information allows to detect differences between cultivars, in plot heterogeneity and crop damages such as lodging. Thus, it holds a great potential for precision agriculture and field-phenotyping applications. Moreover, plant height can be very well estimated for individual dates and across the growing season.

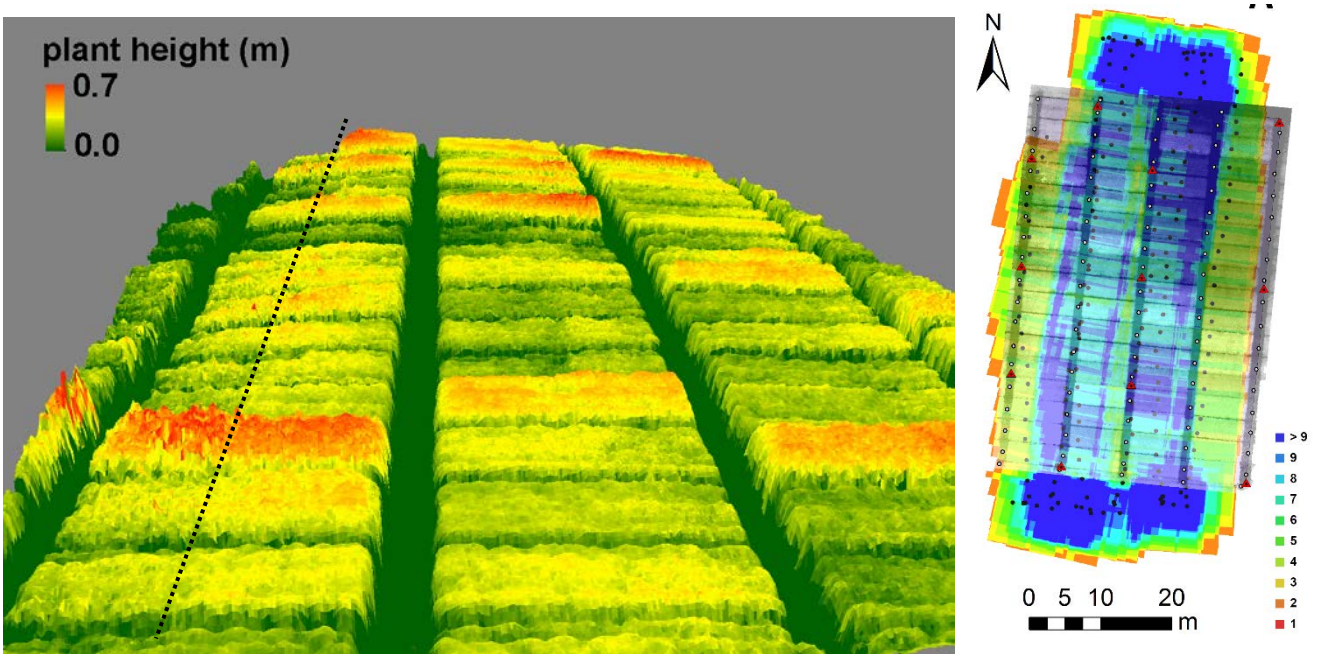

Figure 8 Digital surface model (DSM) colored with the plant height (left) and image overlap (right). On the west side of the most western row (separated with a dashed line), the image overlap is not sufficient for a precise generation of the DSM. Thus, the model becomes noisy and tilts.

Similar, also the spectral data can discriminate between different cultivars and crop damages are visible. Still, the results for the retrieval of chlorophyll are rather weak to moderate. This can be explained by the several influences by which the spectral data is affected. Within an image, every pixel has a different angular composition (Aasen, in-press). Currently, this cannot be corrected for in snapshot imaging data. Thus, angular effects influence the data (Aasen, in review; Aasen and Bolten, in review) and also retrieval methods such as vegetation indices (Burkart et al., 2015; Verrelst et al., 2008). Additionally, at DAS 56 the sky was clouded. Since the current calibration protocol cannot correct for influences due to changing illumination this might have influenced the data. Additionally, under clouded conditions the composition and directionality of incident light is changed compared to clear sky conditions. The current calibration procedure is influenced by this change (Aasen and Bolten, in review). Thus, also the retrieved REIP values are influenced. Additionally, at DAS 56 canopy was not totally closed, which also influenced the relative composition of the red and NIR wavelength of which the REIP is composed. The combination of these effects explain the reduced REIP values at DAS 56 compared to DAS 70 although similar chlorophyll values were measured on leaf level. Thus, while spectral data holds a great potential to estimate a several important parameters for precision agriculture or field-phenotyping, the data needs to be handled with care. In particular, the measurement conditions and metadata about every pixel needs to be provided to fully comprehend the information within each pixel.

Conclusions

A great variety of lightweight imaging sensing systems have lately become availably. Sensors such as the UHD 185-Firefly (www.cubert-gmbh.de), FPI Rikola (http://www.rikola.fi) or Sequoia (http://www.parrot.com) can be carried by UAVs and record spectral and 3D spatial information at the

same time. Still, although data product generation might seem easy in the first place, many details need to be regarded to derive reliable data. This is particularly true for the spectral data, since it is influenced by a multitude of influences. More studies are needed that estimate the influences of these effects on important parameters for precision agriculture and field-phenotyping. Nevertheless, the combination of UAVs and spectral snapshot camera systems hold a great potential to support the need for timely information about agricultural crops.

Acknowledgements

We thank Martin Gynp, Jonas Brands, Simon Bennertz, Janis Broscheit, Markus Drahs, Silas Eichfuss, Sven Ortloff and Maximilian Willkomm very much for their outstanding engagement in the field, and the people of Campus Klein-Altendorf (University of Bonn) for maintaining the field experiment. Additionally, we thank Georg Bareth and Nora Tilly for their support during the preparation of the manuscript. Moreover, we thank Ira Kurth and Mauritio Hunsche (INRES, University of Bonn) for the access to and the support in the laboratory. The field measurements were carried out within CROP.SENSe.net project in the context of the Ziel 2-Programms NRW 2007–2013 ‘‘Regionale Wettbewerbsfähigkeit und Beschäftigung” by the Ministry for Innovation, Science and Research (MIWF) of the state North Rhine Westphalia (NRW) and European Union Funds for regional development (EFRE) (005-1103-0018). We acknowledge Agim Ballvora for the management of the barley cluster within this project. Helge Aasen greatly acknowledges the funding through the fellowship grant of the Graduate School of Geosciences (GSGS-2015B-F01), University of Cologne. We acknowledged Sam Work for proofreading of the manuscript.

References

Aasen, H., in review. The acquisition of hyperspectral digital surface models of crops from UAV snapshot cameras (Dissertation). University of Cologne, Cologne, Germany.

Aasen, H., in-press. Influence of the viewing geometry on hyperspectral data retrieved from UAV snapshot cameras, in: ISPRS Annals of the Photogrammetry, Remote Sensing and Spatial Information Sciences. Presented at the XXIII congress of the International Society for Photogrammetry and Remote Sensing, Prague, Czech Republic.

Aasen, H., Bolten, A., in review. Multi-temporal monitoring of agricultural crops with high-resolution 3D hyperspectral digital surface models in comparison with ground observations.

Aasen, H., Burkart, A., Bolten, A., Bareth, G., 2015. Generating 3D hyperspectral information with lightweight UAV snapshot cameras for vegetation monitoring: From camera calibration to quality assurance. ISPRS J. Photogramm. Remote Sens. 108, 245–259. doi:10.1016/j.isprsjprs.2015.08.002

Aasen, H., Gnyp, M.L., Miao, Y., Bareth, G., 2014. Automated Hyperspectral Vegetation Index Retrieval from Multiple Correlation Matrices with HyperCor. Photogramm. Eng. Remote Sens. 80, 785–795. doi:10.14358/PERS.80.8.785

Agisoft LLC, 2016. Agisoft PhotoScan User Manual Professional Edition, Version 1.2. St. Petersburg, Russia.

Baher, Z.F., Mirza, M., Ghorbanli, M., Bagher Rezaii, M., 2002. The influence of water stress on plant height, herbal and essential oil yield and composition in Satureja hortensis L. Flavour Fragr. J. 17, 275–277. doi:10.1002/ffj.1097

Bendig, J., Bolten, A., Bennertz, S., Broscheit, J., Eichfuss, S., Bareth, G., 2014. Estimating Biomass of Barley Using Crop Surface Models (CSMs) Derived from UAV-Based RGB Imaging. Remote Sens. 6, 10395–10412. doi:10.3390/rs61110395

Bendig, J., Yu, K., Aasen, H., Bolten, A., Bennertz, S., Broscheit, J., Gnyp, M.L., Bareth, G., 2015. Combining UAV-based plant height from crop surface models, visible, and near infrared vegetation indices for biomass monitoring in barley. Int. J. Appl. Earth Obs. Geoinformation 39, 79–87. doi:10.1016/j.jag.2015.02.012

Berni, J., Zarco-Tejada, P.J., Suarez, L., Fereres, E., 2009. Thermal and Narrowband Multispectral Remote Sensing for Vegetation Monitoring From an Unmanned Aerial Vehicle. IEEE Trans. Geosci. Remote Sens. 47, 722–738. doi:10.1109/TGRS.2008.2010457

Blanke, M., 1992. Determination of chlorophyll using DMSO. Wein-Wiss. 47, 32–35.

Broge, N.., Leblanc, E., 2001. Comparing prediction power and stability of broadband and hyperspectral vegetation indices for estimation of green leaf area index and canopy chlorophyll density. Remote Sens. Environ. 76, 156–172. doi:10.1016/S0034-4257(00)00197-8

Burkart, A., Aasen, H., Alonso, L., Menz, G., Bareth, G., Rascher, U., 2015. Angular Dependency of Hyperspectral Measurements over Wheat Characterized by a Novel UAV Based Goniometer. Remote Sens. 7, 725–746. doi:10.3390/rs70100725

Campus Klein-Altendorf, 2010. Standort [WWW Document]. URL https://www.cka.uni-bonn.de/standort (accessed 12.1.16).

Colomina, I., Molina, P., 2014. Unmanned aerial systems for photogrammetry and remote sensing: A review. ISPRS J. Photogramm. Remote Sens. 92, 79–97. doi:10.1016/j.isprsjprs.2014.02.013

Dandois, J.P., Ellis, E.C., 2010. Remote Sensing of Vegetation Structure Using Computer Vision. Remote Sens. 2, 1157–1176. doi:10.3390/rs2041157

Dandois, J.P., Olano, M., Ellis, E., 2015. Optimal Altitude, Overlap, and Weather Conditions for Computer Vision UAV Estimates of Forest Structure. Remote Sens. 7, 13895–13920. doi:10.3390/rs71013895

Daughtry, C.S.T., Walthall, C.L., Kim, M.S., De Colstoun, E.B., McMurtrey, J.E., 2000. Estimating corn leaf chlorophyll concentration from leaf and canopy reflectance. Remote Sens. Environ. 74, 229–239.

DigitalGlobe, 2016. WorldView-3 Satellite Sensor [WWW Document]. WorldView-3 Satell. Imag. Satell. Sens. Specif. Satell. Imaging Corp. URL http://www.satimagingcorp.com/satellite-sensors/worldview-3/ (accessed 4.21.16).

Ehlert, D., Horn, H.-J., Adamek, R., 2008. Measuring crop biomass density by laser triangulation. Comput. Electron. Agric. 61, 117–125. doi:10.1016/j.compag.2007.09.013

Elsayed, S., Rischbeck, P., Schmidhalter, U., 2015. Comparing the performance of active and passive reflectance sensors to assess the normalized relative canopy temperature and grain yield of drought-stressed barley cultivars. Field Crops Res. 177, 148–160. doi:10.1016/j.fcr.2015.03.010

Eltner, A., Schneider, D., 2015. Analysis of Different Methods for 3D Reconstruction of Natural Surfaces from Parallel-Axes UAV Images. Photogramm. Rec. 30, 279–299. doi:10.1111/phor.12115

ESA, 2016. Sentinel-2 MSI - Resolutions [WWW Document]. User Guid. - Sentin.-2 MSI - Resolut. - Sentin. Online. URL https://sentinel.esa.int/web/sentinel/user-guides/sentinel-2-msi/resolutions/spatial (accessed 4.21.16).

FAO (Ed.), 2012. Economic growth is necessary but not sufficient to accelerate reduction of hunger and malnutrition, The state of food insecurity in the world. FAO, Rome.

Foley, J.A., Ramankutty, N., Brauman, K.A., Cassidy, E.S., Gerber, J.S., Johnston, M., Mueller, N.D., O'Connell, C., Ray, D.K., West, P.C., Balzer, C., Bennett, E.M., Carpenter, S.R., Hill, J., Monfreda, C., Polasky, S., Rockström, J., Sheehan, J., Siebert, S., Tilman, D., Zaks, D.P.M., 2011. Solutions for a cultivated planet. Nature 478, 337–342. doi:10.1038/nature10452

Geipel, J., Link, J., Claupein, W., 2014. Combined Spectral and Spatial Modeling of Corn Yield Based on Aerial Images and Crop Surface Models Acquired with an Unmanned Aircraft System. Remote Sens. 6, 10335–10355. doi:10.3390/rs61110335

Gnyp, M.L., Yu, K., Aasen, H., Yao, Y., Huang, S., Miao, Y., Bareth, G., 2013. Analysis of Crop Reflectance for Estimating Biomass in Rice Canopies at Different Phenological Stages. Photogramm. - Fernerkund. - Geoinformation 2013, 351–365. doi:10.1127/1432-8364/2013/0182

Gómez-Gutiérrez, Á., de Sanjosé-Blasco, J., de Matías-Bejarano, J., Berenguer-Sempere, F., 2014. Comparing Two Photo-Reconstruction Methods to Produce High Density Point Clouds and DEMs in the Corral del Veleta Rock Glacier (Sierra Nevada, Spain). Remote Sens. 6, 5407–5427. doi:10.3390/rs6065407

Grenzdörffer, G.J., 2014. Crop height determination with UAS point clouds. ISPRS - Int. Arch. Photogramm. Remote Sens. Spat. Inf. Sci. XL-1, 135–140. doi:10.5194/isprsarchives-XL-1-135-2014

Guyot, N., Baret, F., 1988. Utilisation de la haute resolution spectrale pour suivre l'etat des couverts vegetaux, in: Proceedings of the 4th International Colloquium on Spectral Signatures of Objects in Remote Sensing. Presented at the 4th International Colloquium on Spectral Signatures of Objects in Remote Sensing, NASA Astrophysics Data System, Aussois, France, pp. 279–286.

Haboudane, D., Miller, J.R., Pattey, E., Zarco-Tejada, P.J., Strachan, I.B., 2004. Hyperspectral vegetation indices and novel algorithms for predicting green LAI of crop canopies: Modeling and validation in the context of precision agriculture. Remote Sens. Environ. 90, 337–352. doi:10.1016/j.rse.2003.12.013

Haboudane, D., Miller, J.R., Tremblay, N., Zarco-Tejada, P.J., Dextraze, L., 2002. Integrated narrow-band vegetation indices for prediction of crop chlorophyll content for application to precision agriculture. Remote Sens. Environ. 81, 416–426.

Hagen, N., Kester, R.T., Gao, L., Tkaczyk, T.S., 2012. Snapshot advantage: a review of the light collection improvement for parallel high-dimensional measurement systems. Opt. Eng. 51, 111702–1. doi:10.1117/1.OE.51.11.111702

Harwin, S., Lucieer, A., 2012. Assessing the Accuracy of Georeferenced Point Clouds Produced via Multi-View Stereopsis from Unmanned Aerial Vehicle (UAV) Imagery. Remote Sens. 4, 1573–1599. doi:10.3390/rs4061573

HORSCH Maschinen GmbH, 2016. Leeb GS - product leaflet.

Inoue, Y., Sakaiya, E., Zhu, Y., Takahashi, W., 2012. Diagnostic mapping of canopy nitrogen content in rice based on hyperspectral measurements. Remote Sens. Environ. 126, 210–221. doi:10.1016/j.rse.2012.08.026

Jones, H.G., Vaughan, R.A., 2010. Remote sensing of vegetation: principles, techniques, and applications. Oxford University Press, Oxford ; New York.

Li, F., Miao, Y., Hennig, S.D., Gnyp, M.L., Chen, X., Jia, L., Bareth, G., 2010. Evaluating hyperspectral vegetation indices for estimating nitrogen concentration of winter wheat at different growth stages. Precis. Agric. 11, 335–357. doi:10.1007/s11119-010-9165-6

Mahlein, A.-K., 2016. Plant Disease Detection by Imaging Sensors – Parallels and Specific Demands for Precision Agriculture and Plant Phenotyping. Plant Dis. 100, 241–251. doi:10.1094/PDIS-03-15-0340-FE

Marshall, M., Thenkabail, P., 2015. Developing in situ Non-Destructive Estimates of Crop Biomass to Address Issues of Scale in Remote Sensing. Remote Sens. 7, 808–835. doi:10.3390/rs70100808

Mesas-Carrascosa, F.-J., Torres-Sánchez, J., Clavero-Rumbao, I., García-Ferrer, A., Peña, J.-M., Borra-Serrano, I., López-Granados, F., 2015. Assessing Optimal Flight Parameters for Generating Accurate Multispectral Orthomosaicks by UAV to Support Site-Specific Crop Management. Remote Sens. 7, 12793–12814. doi:10.3390/rs71012793

Milton, E.J., 1987. Principles of field spectroscopy. Int. J. Remote Sens. 8, 1807–1827. doi:10.1080/01431168708954818

Moran, M.S., Inoue, Y., Barnes, E.M., 1997. Opportunities and limitations for image-based remote sensing in precision crop management. Remote Sens. Environ. 61, 319–346. doi:10.1016/S0034-4257(97)00045-X

Mulla, D.J., 2013. Twenty five years of remote sensing in precision agriculture: Key advances and remaining knowledge gaps. Biosyst. Eng. 114, 358–371. doi:10.1016/j.biosystemseng.2012.08.009

Ouédraogo, M.M., Degré, A., Debouche, C., Lisein, J., 2014. The evaluation of unmanned aerial system-based photogrammetry and terrestrial laser scanning to generate DEMs of agricultural watersheds. Geomorphology 214, 339–355. doi:10.1016/j.geomorph.2014.02.016

Pajares, G., 2015. Overview and Current Status of Remote Sensing Applications Based on Unmanned Aerial Vehicles (UAVs). Photogramm. Eng. Remote Sens. 81, 281–330. doi:10.14358/PERS.81.4.281

Pingali, P.L., 2007. Westernization of Asian diets and the transformation of food systems: Implications for research and policy. Food Policy 32, 281–298. doi:10.1016/j.foodpol.2006.08.001

Pinter, P.J.J., Hatfield, J.L., Schepers, J.S., Barnes, E.M., Moran, M.S., Daughtry, C.S.T., Upchurch, D.R., 2003. Remote Sensing for Crop Management. Photogramm. Eng. Remote Sens. 69, 647–664. doi:10.14358/PERS.69.6.647

Pittman, J., Arnall, D., Interrante, S., Moffet, C., Butler, T., 2015. Estimation of Biomass and Canopy Height in Bermudagrass, Alfalfa, and Wheat Using Ultrasonic, Laser, and Spectral Sensors. Sensors 15, 2920–2943. doi:10.3390/s150202920

Remondino, F., Spera, M.G., Nocerino, E., Menna, F., Nex, F., 2014. State of the art in high density image matching. Photogramm. Rec. 29, 144–166. doi:10.1111/phor.12063

Salamí, E., Barrado, C., Pastor, E., 2014. UAV Flight Experiments Applied to the Remote Sensing of Vegetated Areas. Remote Sens. 6, 11051–11081. doi:10.3390/rs61111051

Tilly, N., Aasen, H., Bareth, G., 2015. Fusion of Plant Height and Vegetation Indices for the Estimation of Barley Biomass. Remote Sens. 7, 11449–11480. doi:10.3390/rs70911449

Tilly, N., Hoffmeister, D., Cao, Q., Huang, S., Lenz-Wiedemann, V., Miao, Y., Bareth, G., 2014. Multitemporal crop surface models: accurate plant height measurement and biomass estimation with terrestrial laser scanning in paddy rice. J. Appl. Remote Sens. 8, 83671. doi:10.1117/1.JRS.8.083671

Tilman, D., Balzer, C., Hill, J., Befort, B.L., 2011. Global food demand and the sustainable intensification of agriculture. Proc. Natl. Acad. Sci. 108, 20260–20264. doi:10.1073/pnas.1116437108

Verrelst, J., Schaepman, M.E., Koetz, B., Kneubühler, M., 2008. Angular sensitivity analysis of vegetation indices derived from CHRIS/PROBA data. Remote Sens. Environ. 112, 2341–2353. doi:10.1016/j.rse.2007.11.001

Whelan, B., Taylor, J., 2013. Precision agriculture for grain production systems. CSIRO Publishing, Collingwood, Vic.

Yao, H., Tang, L., Tain, L., Brown, R.L., Bhatnagar, D., Cleveland, T.E., 2012. Using Hyperspectral Data in Precision Farming Applications, in: Thenkabail, P.S., Lyon, J.G., Huete, A. (Eds.), Hyperspectral Remote Sensing of Vegetation. CRC Press, Boca Raton, FL, pp. 591–608.

Yu, K., Lenz-Wiedemann, V., Chen, X., Bareth, G., 2014. Estimating leaf chlorophyll of barley at different growth stages using spectral indices to reduce soil background and canopy structure effects. ISPRS J. Photogramm. Remote Sens. 97, 58–77. doi:10.1016/j.isprsjprs.2014.08.005

Yu, K., Leufen, G., Hunsche, M., Noga, G., Chen, X., Bareth, G., 2013. Investigation of Leaf Diseases and Estimation of Chlorophyll Concentration in Seven Barley Varieties Using Fluorescence and Hyperspectral Indices. Remote Sens. 6, 64–86. doi:10.3390/rs6010064